


Enzymatic Degradation of A2E, a Retinal Pigment Epithelial Lipofuscin Bisretinoid

Yalin Wu,[†] Jilin Zhou,[†] Nathan Fishkin,[§] Bruce E. Rittmann,^{||} and Janet R. Sparrow^{*,†,‡}

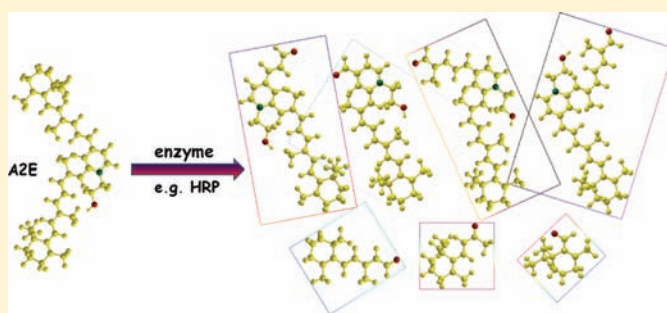
[†]Department of Ophthalmology and [‡]Department of Pathology and Cell Biology, Columbia University, 630 West 168th Street, New York, New York 10032, United States

[§]ImmunoGen, Incorporated, Waltham, Massachusetts 02451-1477, United States

^{||}Center for Environmental Biotechnology, Biodesign Institute of Arizona State University, Tempe, Arizona 85287-5701, United States

 Supporting Information

ABSTRACT: Some forms of blinding macular disease are associated with excessive accumulation of bisretinoid lipofuscin in retinal pigment epithelial (RPE) cells of the eye. This material is refractory to lysosomal enzyme degradation. In addition to gene and drug-based therapies, treatments that reverse the accumulation of bisretinoid would be beneficial. Thus, we have examined the feasibility of degrading the bisretinoids by delivery of exogenous enzyme. As proof of principle we report that horseradish peroxidase (HRP) can cleave the RPE bisretinoid A2E. In both cell-free and cell-based assays, A2E levels were decreased in the presence of HRP. HRP-associated cleavage products were detected by ultraperformance liquid chromatography (UPLC) coupled to electrospray ionization mass spectrometry, and the structures of the aldehyde-bearing cleavage products were elucidated by ¹⁸O-labeling and ¹H NMR spectroscopy and by recording UV–vis absorbance spectra. These findings indicate that RPE bisretinoids such as A2E can be degraded by appropriate enzyme activities.



INTRODUCTION

Beginning in childhood, retinal pigment epithelial (RPE) cells in the eye accumulate fluorescent compounds that constitute the lipofuscin of the cell. These pigments are derived from reactions of all-*trans*-retinal, the retinoid that is generated when 11-*cis*-retinal, the chromophore of visual pigment, isomerizes after absorbing a photon of light. Several bisretinoid pigments have been identified in RPE lipofuscin including A2E (Figure 1g and Supporting Information Figure S1) and its isomers, A2-dihydropyridine-phosphatidylethanolamine (A2-DHP-PE), and compounds of the all-*trans*-retinal dimer series (all-*trans*-retinal dimer, all-*trans*-retinal dimer-ethanolamine, all-*trans*-retinal dimer-phosphatidylethanolamine).¹ The nonenzymatic biosynthetic pathways leading to the formation of these bisretinoids have been elucidated, at least in part, and for all of these bisretinoids, biosynthesis begins in photoreceptor cells.^{1a,2} When discarded photoreceptor outer segments are phagocytosed by RPE cells, the bisretinoid precursors are deposited into the lysosomal compartment of the cells. An enzyme activity that has been shown to be phospholipase-D and to be present in RPE cell lysosomes can remove phosphatidic acid from the bisretinoid precursors; as a result, A2E is released from A2PE and all-*trans*-retinal dimer-ethanolamine from all-*trans*-retinal dimer-phosphatidylethanolamine.^{1b,2a,3} However, after this enzyme-mediated phosphate cleavage, little or no further

enzyme degradation of the bisretinoid molecules occurs; thus, the pigment accumulates in the cell. We surmise that, since the structure of A2E is unprecedented, it may not be recognized by other lysosomal enzymes of the RPE and, thus, is largely indigestible.³

In addition to the age-related accumulation, RPE lipofuscin forms in particular abundance in retinal disorders caused by mutations in *ABCA4* (formerly *ABCR*),⁴ the gene that encodes a photoreceptor-specific ATP-binding cassette transporter.⁵ Indeed, evidence on several fronts indicates that the excessive accumulation of this material in RPE cells is responsible for the retinal degeneration that characterizes *ABCA4*-related disorders including Stargardt macular degeneration, retinitis pigmentosa, and cone–rod dystrophy.⁶ Elevated levels are also observed in mouse models that mimic ELOVL-4-related autosomal dominant macular dystrophy⁷ and deficiencies in members of the retinol dehydrogenase family of enzymes.⁸ The bisretinoid compounds of RPE lipofuscin may also contribute to complement activation,⁹ dysregulation of which may be the basis for the associations between genetic variants in complement factors and susceptibility to age-related macular degeneration.¹⁰

Received: August 10, 2010

Published: December 17, 2010

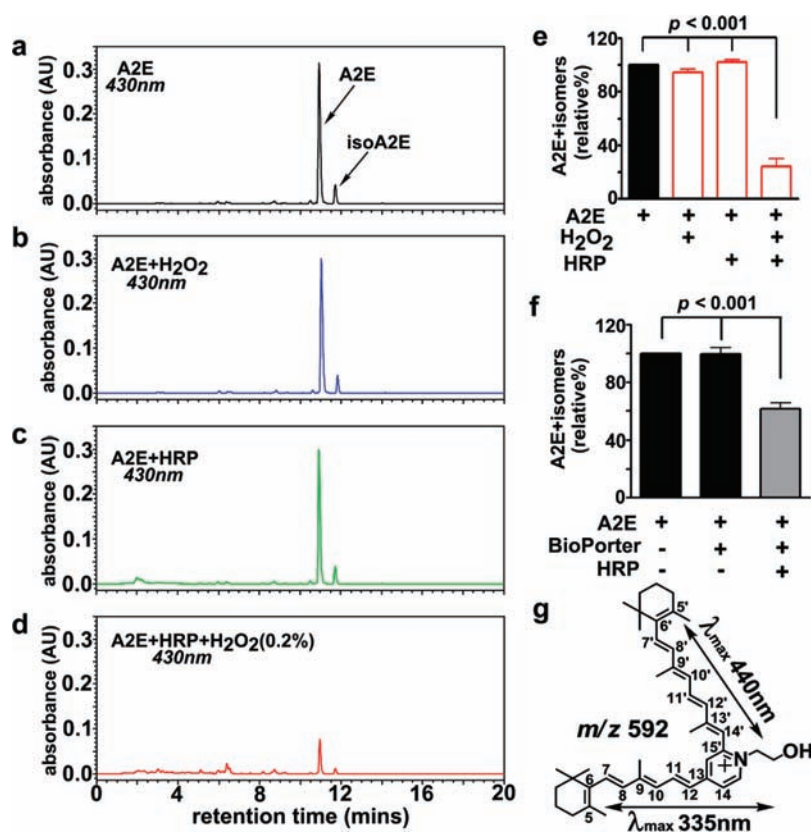


Figure 1. HPLC quantitation of A2E pigment after incubation in the presence and absence of horseradish peroxidase (HRP)/H₂O₂. (a–d) HPLC chromatograms generated with samples of A2E, A2E incubated with H₂O₂, A2E incubated with HRP, and A2E incubated with H₂O₂ (0.2%) and HRP for 24 h; reversed-phase HPLC. (e) Quantitation of A2E and A2E isomers. Chromatographic peak areas were measured, A2E and isomers were summed and are presented as percent of pigment in the absence of HRP and H₂O₂; mean \pm SEM of three experiments; +, presence of compound/reagent. HPLC quantitation of A2E in ARPE-19 cells to which HRP was delivered using Bioporter reagent; +, presence of compound/reagent; mean \pm SEM of 4–7 experiments. (f) HPLC quantitation of A2E in ARPE-19 cells to which HRP was delivered using Bioporter reagent; +, presence of compound/reagent. Values (pmol/10⁶ cells) are expressed as percent of A2E in absence of Bioporter and HRP; mean \pm SEM of 4–7 experiments. (g) A2E: structure, mass-to-charge ratio (m/z), UV–vis absorbance (nm), and electronic transition assignments (\leftrightarrow).

Therapeutic approaches aimed at alleviating vision loss in *ABCA4*-associated disease have shown that lipofuscin bisretinoid formation can be retarded. These approaches have included gene therapies based on viral vector mediated delivery of the wild-type gene¹¹ and systemic administration of compounds that limit the retinoid cycle so as to decrease all-*trans*-retinal formation.¹² Nevertheless, neither gene nor drug therapy can reverse the accumulation of lipofuscin bisretinoids such as A2E, once it has already occurred. Thus, in *in vitro* experiments described here, we have tested an additional treatment method. Specifically, we sought to determine whether enzymes can be delivered to RPE cells for the purpose of safely degrading the bisretinoid constituents of RPE lipofuscin. As proof of principle, we employed a well-known enzyme, horseradish peroxidase (HRP). HRP is one of a group of oxo–iron heme based enzymes that also include cytochrome P450, chloroperoxidase, cytochrome *c* peroxidase, and catalase. On the basis of noncellular and cell-based assays and by employing quantitative HPLC (high-performance liquid chromatography), UPLC–MS (ultraperformance liquid chromatography–mass spectrometry), and NMR (nuclear magnetic resonance) spectroscopy, we have demonstrated enzymatic degradation of A2E.

RESULTS

HRP Degrades A2E in a Cell-Free Assay. We first probed for evidence that HRP can act on A2E by incubating HRP and A2E in

a cell-free system with and without H₂O₂. Shown in Figure 1a–d are representative HPLC chromatograms generated from various mixtures of A2E, HRP, and H₂O₂. Quantitation by integrating peak areas (Figure 1e) demonstrated that after a 24 h incubation with HRP and H₂O₂, levels of A2E in the mixture were reduced by 75% relative to starting levels. HRP or H₂O₂ alone did not diminish A2E (Figure 1, parts b, c, and e). Interestingly, the peaks attributable to A2E and iso-A2E were often bifurcated after HRP incubation, suggesting that the compounds had been modified, such as by oxidation. Cathepsin D is a ubiquitous lysosomal enzyme that is known to play a role in the lysosomal digestion of phagocytosed photoreceptor outer segments by RPE cells.¹³ In contrast to the effects observed with HRP and H₂O₂ wherein incubation for 5 h resulted in decreases in A2E levels (Supporting Information Figure S2b), no changes were observed when A2E was incubated with cathepsin D (Supporting Information, Figure S2c–e) at either pH 5.0 or 6.5. To determine whether lysosomal conditions are optimal for HRP-mediated degradation of A2E, we also incubated the latter bisretinoid with HRP at varying pH values (Figure 2). We found that A2E degradation was considerably increased at pH 5.5 versus pH 7.2 and pH 6.5. Lysosomal pH is typically \sim 5.5.

HRP and A2E in a Cell-Based Assay. We delivered HRP to ARPE-19 cells in culture by employing the Bioporter system, an approach that uses a lipid-based reagent to encapsulate molecules,

thus forming complexes that attach to negatively charged cell surfaces and are internalized. To confirm uptake of HRP, we fixed and permeabilized the cells, immunostained with antibodies to HRP, and detected labeling using a chromagen that can be visualized with both fluorescence and bright field microscopy. As shown in Figure 3, parts a and b, 3 days after exposing the cells to Bioporter/HRP, HRP-specific immunoreactivity was observed in association with all of the cells in the cultures.

We have previously shown that, when A2E accumulates in cultured RPE, the pigment is deposited into the lysosomal compartment.¹⁴ As for the fate of protein delivered by the Bioporter system, it has been reported that uptake into cells leads to an endosomal, cytosolic, and nuclear distribution of the carried protein;¹⁵ in addition, lysosomal deposition is indicated by studies

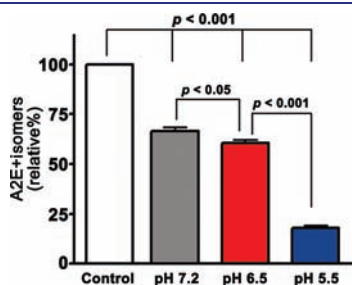


Figure 2. Effects of pH on HRP-mediated degradation of the bisretinoid A2E. A2E (20 μ M) was incubated with HRP (200 units/mL) and H₂O₂ (0.6%) at the indicated pH for 5 h or was incubated in the absence of HRP/H₂O₂. Residual A2E and isomers were quantified by reversed-phase HPLC. Mean \pm SEM of three experiments.

showing that the degradation of proteins delivered into the cell by Bioporter is reduced by inhibitors of lysosomal proteolytic activity.¹⁶ Thus, to determine whether HRP, when delivered to the cells in our experiments, is also located in lysosomes, we sought evidence for colocalization of HRP and a lysosomal probe, Lysotracker Red, a membrane-diffusible acidophilic fluorophore. To this end, ARPE-19 cells that had acquired intracellular HRP were incubated with Lysotracker Red, fixed, and immunostained for HRP. On examination by confocal microscopy, colocalization of HRP and Lysotracker Red was evident from the merging of red (Lysotracker) and green (HRP) signals to yield yellow (Figure 3d–g). These results indicated that at least a portion of the HRP taken up into the cells resided within lysosomes.

To test for the ability of the internalized HRP to degrade A2E, we first allowed ARPE-19 cells to accumulate A2E in culture, withdrew A2E from the media, waited 7 days, and then delivered HRP via the Bioporter system. Three days after introducing HRP to the cultures, we harvested the cells and quantified A2E by HPLC (Figure 1f). In cells that had been incubated with Bioporter and HRP, A2E levels were reduced by \sim 40% as compared to Bioporter alone. After 7 and 14 days, the decrease was not appreciably different (range, 35–45%). Bioporter in the absence of HRP conferred no changes in A2E levels (Figure 1f), indicating that HRP is exclusively responsible for the degradation and oxidation of A2E.

Effects of HRP-Mediated Degradation of Intracellular A2E on Cell Viability. We assayed the health of ARPE-19 cells in the presence of HRP-mediated A2E cleavage. In these experiments we took ARPE-19 cells that had accumulated A2E in culture and

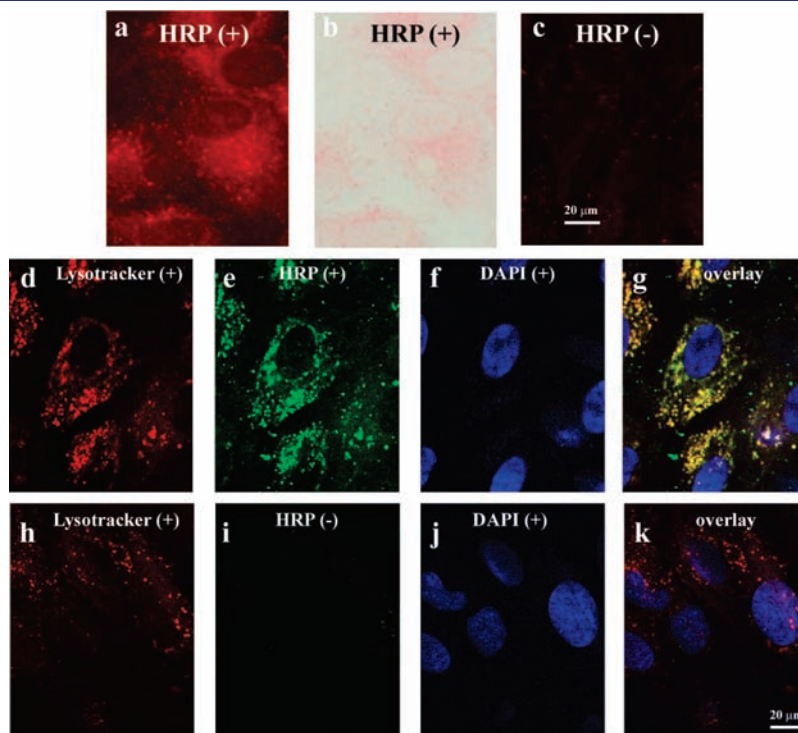


Figure 3. Intracellular horseradish peroxidase (HRP) delivered to ARPE-19 cells accumulated in lysosomes. (a–c) Intracellular horseradish peroxidase introduced to the cells via Bioporter delivery is detected immunocytochemically using primary antibody to HRP, an avidin–biotin–alkaline phosphatase complex, and color development with Vector Red. The reaction product is visible with both fluorescence (a) and bright field (b) optics. HRP is present (+) or absent (–). (d–k) Colocalization of HRP with a lysosomal marker in ARPE-19 cells. Imaging by laser scanning confocal microscopy (x – y scans). Lysotracker (d and h), HRP present (+) or absent (–) (e and i), DAPI-stained nuclei (f and j), and overlay (g and k).

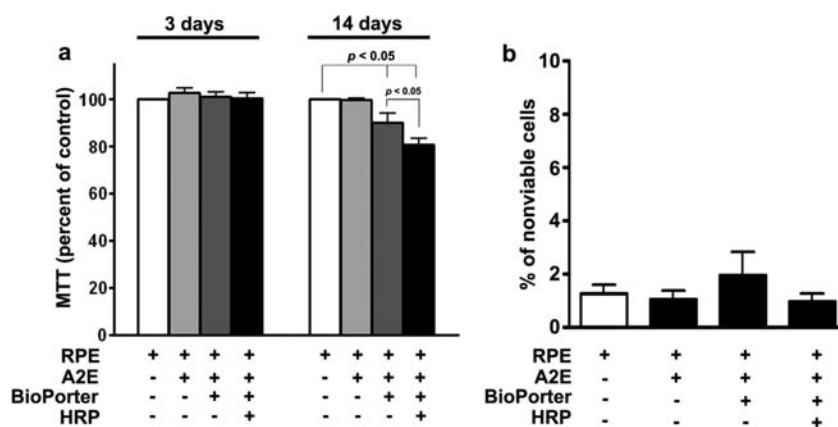


Figure 4. Cell viability with HRP-mediated degradation of intracellular A2E. (a) Cell viability 3 and 14 days after introduction of HRP was probed by MTT assay. Bar height is indicative of MTT absorbance (at 570 nm) and reflects cell viability; mean \pm SEM of four experiments. (b) A two-color fluorescence assay was employed to quantify percent nonviable cells; mean \pm SEM of two experiments. Cells accumulated A2E in culture, and HRP was delivered to the cells using Bioporter reagent; +, presence of compound/reagent.

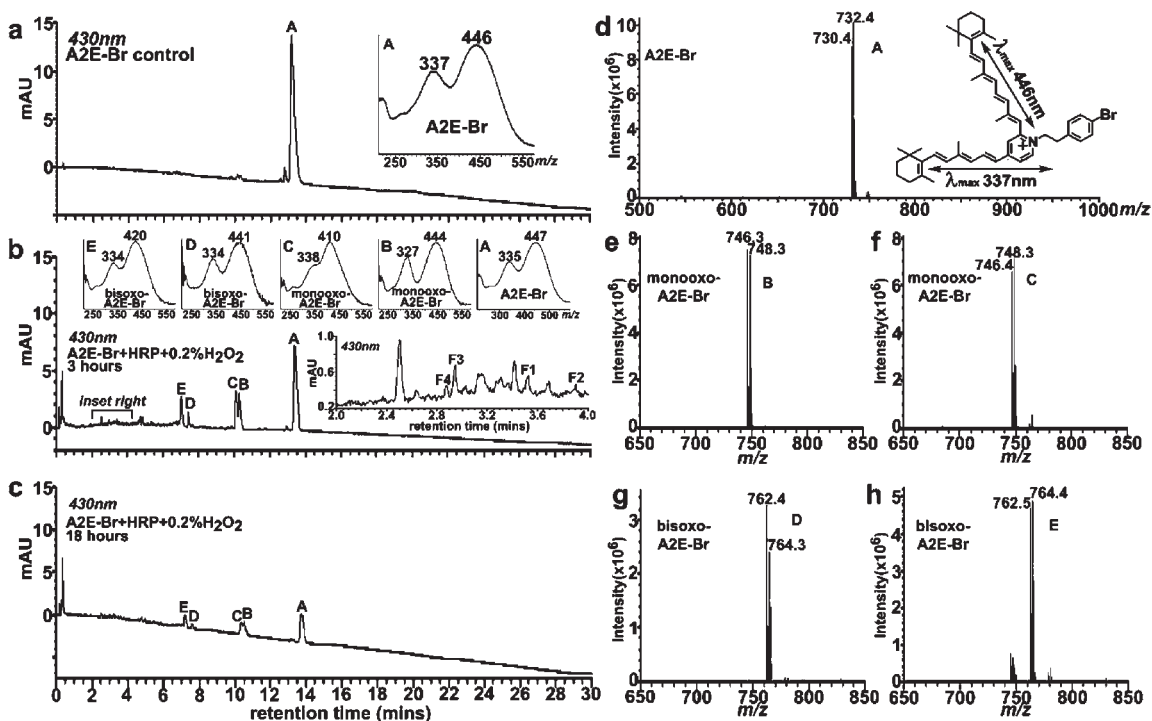


Figure 5. UPLC-ESI-MS analysis of samples of A2E-bromine (A2E-Br) following oxidation and cleavage by horseradish peroxidase (HRP). (a-c) Representative reversed-phase UPLC profiles (Acquity BEH C18 column, monitoring at 430 nm) obtained after 3 and 18 h incubations of A2E-Br, HRP, and H₂O₂ (0.2%), and A2E-Br alone. Insets in panels a and b (top): UV-vis absorbance spectra of A2E-Br, mono-oxo-A2E-Br, and bis-oxo-A2E-Br. Inset in panel b (right): chromatogram expanded between retention time 2–4 min for detection of HRP-associated cleavage products (F1–F4); the chromatogram is magnified in Figure 6a. (d–h) MS spectra of peaks a–e present in panels a–c. The molecular ions at m/z 730/732, 746/748, and 762/764 correspond to A2E-Br, mono-oxo-A2E-Br, and bis-oxo-A2E-Br, respectively. Note bromine isotope (⁷⁹Br and ⁸¹Br) peaks differing by 2 m/z units in panels d–h. Inset in panel d: A2E-Br structure, UV-vis absorbance (nm), and electronic transition assignments (\leftrightarrow).

delivered HRP via the Bioporter system. Three and 14 days after introducing HRP to the cultures, we quantified A2E by HPLC and in companion cultures assayed cell viability by MTT assay. In cells that had been incubated with Bioporter and HRP, A2E levels were reduced by \sim 40% versus incubation with Bioporter only. A concomitant loss of cell viability was not observed within 3 days, since MTT absorbance readings in cultures that had accumulated A2E versus cultures that had accumulated both A2E and HRP were not significantly different (Figure 4a). After

3 days, loss of cell viability was also not observed with a fluorescence assay (Figure 4b). However, after 14 days, cell viability by MTT assay was decreased by 10.5% as compared to cultures receiving Bioporter without HRP (Figure 4a). When cultures were compared by MTT assay 7 and 14 days after HRP delivery, cell viability was decreased by 10% and 8%, respectively (data not shown).

UPLC-MS Detection of A2E Degradation. Since quantitative HPLC analysis indicated that A2E could serve as a substrate

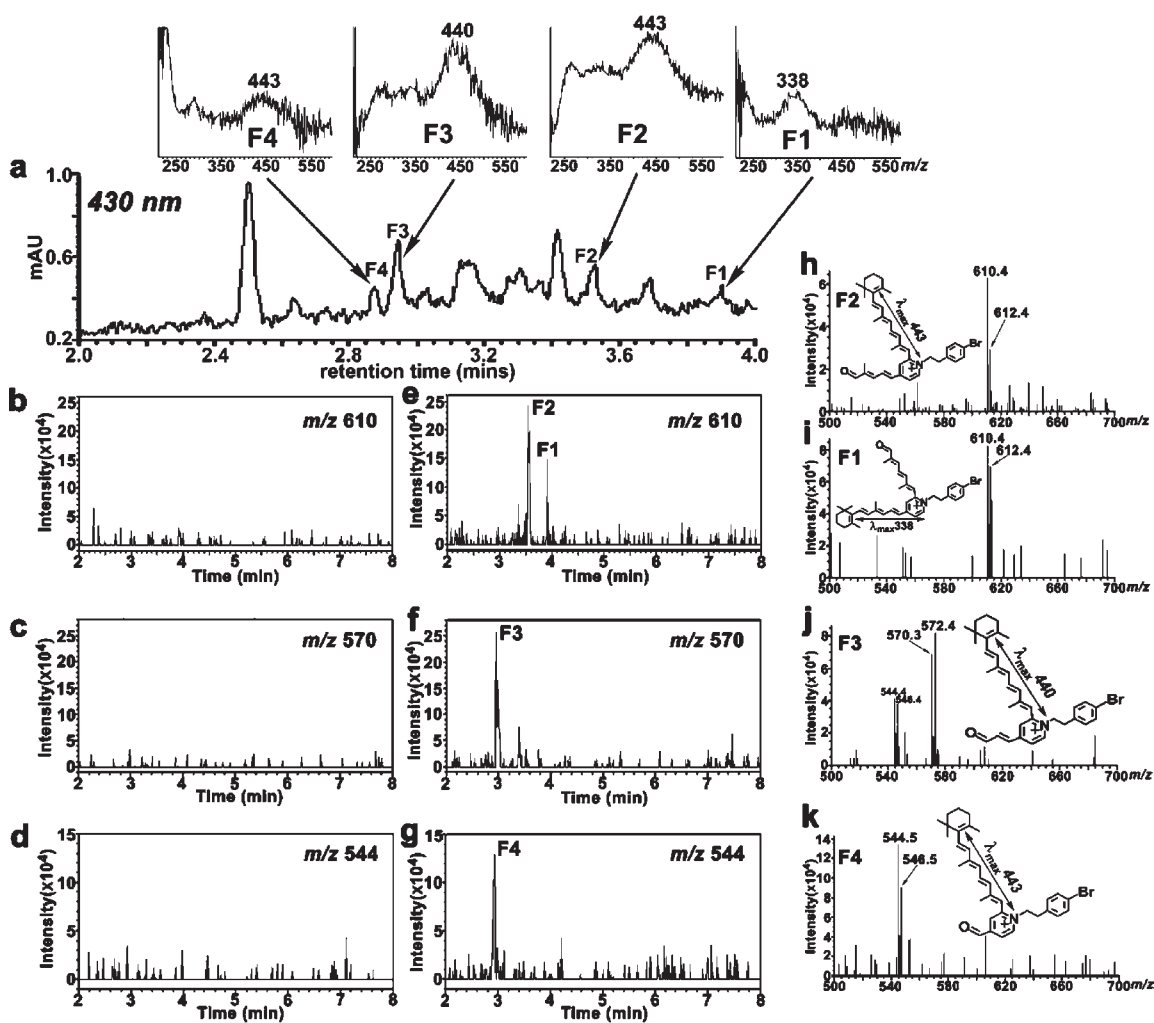


Figure 6. UPLC–MS analysis of HRP-induced cleavage products of A2E-Br. (a) UPLC chromatogram (monitoring at 430 nm) of A2E-Br incubated with HRP and H_2O_2 (0.2%) for 3 h; expanded between retention times 2–4 min (full chromatogram in Figure 5b). Top insets: UV–vis absorbance spectra of cleavage products F1–F4. (b–g) Extracted ion monitoring chromatograms of A2E-Br incubated in water (b–d) and with HRP and H_2O_2 (e–g) for 3 h. Data were acquired in ESI mode with selection for mass-to-charge ratios (m/z) 610, 570, and 544 and recorded as a function of retention time in a reversed-phase UPLC column. In panels e–g four prominent ion peaks corresponding to UPLC peaks F1–F4 (panel a) were observed. (h–k) Assignment of m/z to chromatographic peaks (F1–F4) by coupled electrospray ionization analyses. The bromine tag was indicative of cleavage products that included the pyridinium headgroup of A2E-Br. Insets: proposed structures of cleavage products and electronic transition assignments (\leftrightarrow) of intact arms of A2E-Br.

for HRP, we also sought to determine whether the enzyme activity resulted in both oxidation and cleavage of A2E. To facilitate the detection of oxidation and cleavage products, A2E-Br (Supporting Information Figure S1 and Figure 5d) was used. The bromine tag in this analogue imparts a characteristic isotope pattern (two peaks of similar intensity separated by 2 m/z units due to isotopes ^{79}Br and ^{81}Br) that makes the signal in the mass spectrum more readily distinguishable. Thus, molecular ions featuring the bromine isotope peaks could be recognized as cleavage products that contained the pyridinium headgroup of A2E-Br. Accordingly, UPLC chromatograms of A2E-Br incubated with HRP and H_2O_2 for 3 h exhibited four prominent peaks (Figure 5b, peaks B–E) and several minor peaks (Figure 5b, inset, e.g., F1–F4) that were not present in the sample of A2E-Br incubated in the absence of HRP (Figure 5a). These peaks eluted earlier than A2E-Br (Figure 5a–c, peak A) and thus are consistent with oxidized and cleaved products that are more polar than the parent compound.¹⁷ Subsequent analysis

of the prominent UPLC peaks (Figure 5b, peaks B–E) by coupled mass spectrometry revealed ion signals with $m/z + 16$ (B, 746/748; C, 746/748) and $m/z + 2 \times 16$ (D, 762/764; E, 762/764) (Figure 5e–h), relative to A2E-Br (m/z 730/732) (Figure 5d). These peaks were indicative of the addition of one (Figure 5b, peaks B and C) and two oxygen atoms (Figure 5b, peaks D and E). Following an 18 h incubation period, the heights of the peaks corresponding to oxidized A2E-Br were significantly diminished, suggesting cleavage of these species (Figure 5, part c versus b).

From our earlier work,¹⁸ we anticipated that loss of a carbon–carbon double bond ($\text{C}=\text{C}$) due to oxidation on the long arm of A2E-Br would result in a blue-shift (25–40 nm) of the longer wavelength absorbance of A2E-Br (λ_{max} 446 nm), whereas oxidation on the short arm would shift the shorter wavelength absorbance (λ_{max} 337 nm). Accordingly, two oxidized species (Figure 5b, peak C, λ_{max} 338 and 410 nm; Figure 5b, peak E, λ_{max} 334 and 420 nm) presented with longer

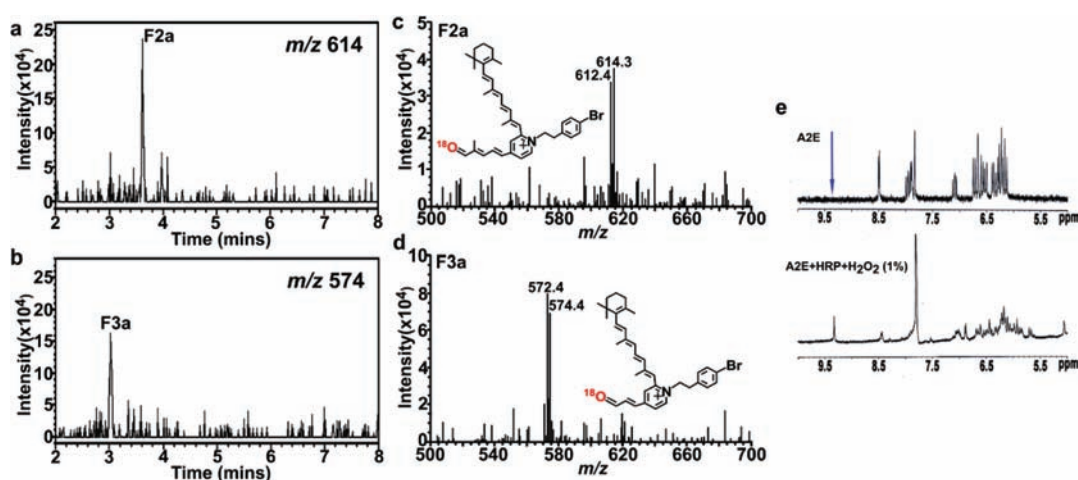


Figure 7. Elucidation of aldehyde-containing cleavage products. (a–d) UPLC–MS analysis of ^{18}O -labeled cleavage products generated from A2E-Br incubated with HRP in ^{18}O -labeled water (H_2^{18}O) and hydrogen peroxide ($\text{H}_2^{18}\text{O}_2$). (a and b) Selected ion chromatograms with detection set for mass-to-charge ratios (m/z) of 614 and 574. Two peaks (F2a and F3a) were observed that corresponded to ^{18}O -labeled peaks F2 and F3 according to the identical retention time. (c and d) ESI-MS spectra of the chromatographic peaks, F2a and F3a. Insets: structures of ^{18}O -labeled cleavage products. In the use of H_2^{18}O and $\text{H}_2^{18}\text{O}_2$, the mass of F2 (m/z 610/612) and F3 (m/z 570/572) is shifted by 2 m/z units to 612/614 (F2a) and 572/574 (F3a), respectively, due to ^{16}O – ^{18}O exchange. (e) ^1H NMR spectra recorded in the region of 10–5 ppm (400 MHz; MeOD): upper, A2E; lower, A2E incubated with HRP and H_2O_2 for 5 h. The signal at ~ 9.4 ppm (arrow) is characteristic of the aldehyde proton.

wavelength absorbances that were blue-shifted relative to A2E-Br, indicating epoxidation at one $\text{C}=\text{C}$ on the long arm. The second of these oxidized products (Figure 5b, peak E) had a mass of 762/764 indicating the addition of two oxygen atoms; yet, since the long-arm absorbance shift indicated a loss of only one $\text{C}=\text{C}$ bond, hydroxylation of one methyl moiety was considered to account for the second oxygen atom. Similarly, since the UV–vis absorbances of two other oxidized products (Figure 5b, peak B, λ_{max} 327 and 444 nm; Figure 5b, peak D, λ_{max} 334 and 441 nm) were similar to that of A2E-Br (λ_{max} 337 and 446 nm) (Figure 5a) it is likely that these compounds had undergone methyl hydroxylation (see Figure 8) not $\text{C}=\text{C}$ bond epoxidation. Hydroxylation of a methyl moiety is unlikely to have an appreciable effect on UV–vis absorbance.

Several minor peaks (Figure 5b) eluted earlier than the oxidized products discussed above; four of these were examined (Figure 5b, inset, F1–F4; Figure 6a). As shown in Figure 6e–g, extracted ion chromatograms with selection for mass-to-charge ratios (m/z) 610, 570, and 544 revealed four prominent ion chromatographic peaks that, on the basis of retention time, corresponded to UPLC peaks F1–F4 (Figure 6a). These ion chromatographic peaks were not observed in samples of A2E-Br incubated in the absence of HRP (Figure 6b–d). Analysis of UPLC peaks F1–F4 by electrospray ionization mass spectrometry (ESI-MS) (Figure 6h–k) corroborated the presence of ion signals at m/z 610/612 (F1 and F2), 570/572 (F3), and 544/546 (F4); all were lower in mass than m/z 730/732 attributable to A2E-Br (Figure 5d) and thus were indicative of HRP-induced cleavage products. These A2E cleavage products were not visible after incubation for 18 h (Figure 5c) probably because of further HRP-mediated degradation.

^{16}O – ^{18}O Exchange. To further elucidate reaction mechanisms involved in HRP-mediated A2E cleavage, we utilized oxygen isotope labeling to determine the number of oxygen atoms added to the cleavage products. To this end, we incubated A2E-Br with HRP in ^{18}O -labeled water (H_2^{18}O) in the presence of ^{18}O -labeled hydrogen peroxide ($\text{H}_2^{18}\text{O}_2$) for 18 h and monitored relevant cleavage products by UPLC–MS. As depicted in

Figure 7, selected ion monitoring at m/z 614 and 574 to detect the heavy isotope (+2 m/z units) revealed prominent ion chromatographic peaks, F2a (Figure 7a) and F3a (Figure 7b), indicative of the inclusion of ^{18}O in the cleavage product. Examination of these two ion chromatographic peaks (F2a and F3a) by ESI-MS divulged m/z signals at 612/614 for F2a (Figure 7c) and 572/574 for F3a (Figure 7d). Again the +2 m/z units (m/z 610/612 for F1/F2 and m/z 570/572 for F3) verified the presence of one ^{18}O atom in each A2E-Br cleavage product. Since the ^{16}O – ^{18}O exchange does not alter retention time, we could readily identify compounds F2a (Figure 7c, inset) and F3a (Figure 7d, inset) as being the same as F2 and F3, respectively. ^{18}O -labeled species (m/z 612/614 and 546/548) corresponding to cleavage products F1 and F4 (m/z 610/612 and 544/546, respectively) were not observed. Note that some inefficiency of $\text{H}_2^{18}\text{O}_2$ labeling can be expected since the heavy isotope reacts more sluggishly and $\text{H}_2^{16}\text{O}_2$ is present as 10%.

NMR Detection of Aldehyde Moiety. After incubating A2E with HRP and H_2O_2 at 37 °C for 5 h, ^1H NMR spectroscopy revealed a new resonance at 9.0–9.5 ppm indicative of a specific aldehyde proton signal that was not present with untreated A2E (Figure 7e). This finding is indicative of the generation of aldehyde moieties. Aldehydes would form subsequent to enzyme catalyzed oxidation of A2E-Br at double bonds along the polyene chains, followed by cleavage.

Assignments of Cleavage Structures. Structures were proposed for the cleavage products F1–F4 (Figure 5b, insets; Figure 6a; Figure 6h–k, insets) on the basis of m/z values together with data from the NMR and oxygen isotope studies indicating cleavage products bearing a single oxygen atom residing within an aldehyde moiety. In addition, we could be certain that the bromine isotope peaks signaled the presence of the pyridinium ring in the A2E-Br fragment. We found that both acyclic polyenic side arms of A2E-Br were susceptible to HRP-mediated epoxidation, hydroxylation, and degradation. For instance, two of the ion peaks, specifically F1 and F2 (m/z 610/612), presented with the same mass but different retention times because of cleavage on the short (F2) versus long

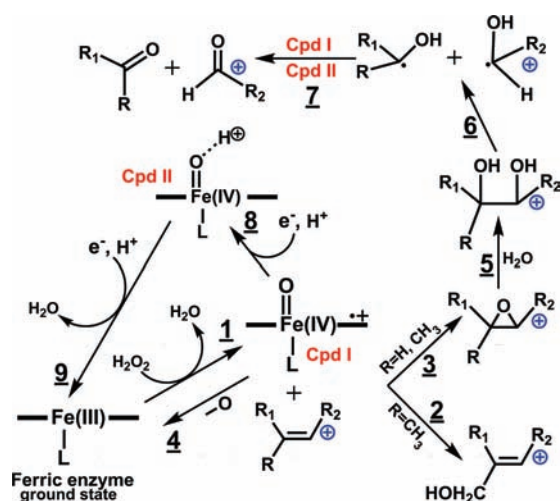


Figure 8. Proposed mechanisms for HRP-catalyzed oxidation and degradation of A2E; L, ligand. The HRP catalytic cycle involves two active species, compound I (Cpd I) and compound II (Cpd II), that possess high-valence iron ions storing two and one oxidation equivalents, respectively (ref 31). Two-electron oxidation of HRP by H_2O_2 (step 1) generates the first active species Cpd I; the latter mediates oxygen-transfer reactions to yield C–H hydroxylation (step 2) and/or C=C epoxidation (step 3). Cpd I then returns to ground state (step 4). At epoxidation sites, opening and hydration of the epoxide ring would give rise to a diol (step 5) that would undergo a periodate-like enzymatic carbon–carbon fission reaction to form two carbon-centered alcoholic radicals (step 6), one that includes the positively charged pyridinium ring (\oplus) with the residual component being without charge (neutral) (step 6). Cpd I (step 1) initiates one-electron oxidation on one of these radicals to generate an aldehyde or methylketone-bearing products (step 7) and Cpd II (step 8). The latter forms by transfer of a hydrogen atom from the hydroxyl group of the radical to the iron–oxo complex (Cpd I). Subsequently one-electron oxidation of another radical by Cpd II yields an aldehyde or methylketone-bearing product (step 7), and the enzyme (Cpd II) returns to ground state (ref 19) (step 9). Note that enzyme cleavage at the 9–10 double bond would generate an aldehyde-bearing fragment and a ketone-bearing fragment; cleavage at 7–8, 7′–8′, or 11′–12′ double bonds would lead to two aldehyde-bearing fragments.

arm (F1). This was deduced from the UV–vis absorbance spectra (Figure 6),¹⁸ whereby both the F1 and F2 cleavage products exhibited single absorbance maxima (Figure 6), with F1 lacking the longer wavelength absorbance, whereas F2 was missing the short-wavelength absorbance of A2E-Br. Thus, F1 would have resulted from epoxidation and cleavage at the C7, C8 (short arm) bond, whereas F2 would follow from the same process at the C7′, C8′ (long arm) double bond (Figure 6). By the mechanism shown in Figure 8, cleavage at these sites would release a pair of aldehyde-bearing products,¹⁹ F1 or F2 and 2,6,6-trimethylcyclohex-1-enecarbaldehyde (Supporting Information Figure S3). The latter is a small and volatile aldehyde-bearing compound that would be difficult to detect by direct LC–MS without trapping.¹⁷ The HRP-catalyzed pathways for formation of ion signals at m/z 570/572 and 544/546 attributable to cleavage products F3 and F4, respectively (Figure 6), were similar to that of F1 and F2. The minor differences were that epoxidation sites of the parent compound were at the C9–C10 and C11–C12 double bonds, respectively.

DISCUSSION

We have shown here that A2E, a compound that contains multiple C=C functionalities, can serve as a substrate for HRP-mediated

oxidation and degradation, and we propose a mechanism by which this would occur (Figure 8). Importantly, as has been shown previously for other substrates,²⁰ HRP can act on A2E at pH 5.5, the pH of lysosomes wherein the bisretinoids of RPE reside. We have characterized the structures of four of the largest degradation products; continued decline with time in the peak intensities attributable to these products indicated that enzyme-mediated cleavage was progressive. In our acellular assays, the addition of H_2O_2 was a corequisite to HRP-mediated A2E cleavage. However, in our cell-based experiments since exogenous H_2O_2 was not added, it is likely that mitochondrial metabolism served as a source of H_2O_2 . Of course HRP is an enzyme that RPE cells would not normally produce. We observed that 3 days after the introduction of HRP to the cells, A2E levels were reduced by approximately 40%. At longer intervals (7 and 14 days) no further decrease was observed. This limited period of degradation may reflect the lifetime of the enzyme under intracellular conditions and could be an advantage since persistence of the therapeutic enzyme longer than required may be undesirable. Measured as a decline in amounts of A2E, the therapeutic effect observed with small molecules that target the visual cycle in mouse models have ranged from 30% to 60%.^{12a,b,21}

HRP can mediate at least two oxygen-transfer reactions: C–H hydroxylation of alkanes and C=C epoxidation of alkenes.²² Since the side arms of A2E consist of alternating carbon–carbon double bonds together with methyl groups, it follows that HRP/ H_2O_2 mediated oxidation of A2E would involve both hydroxylation of methyl groups and epoxidation of C=C double bonds. It has previously been noted that HRP-mediated epoxidation is frequently followed by the formation of aldehydes.²³ Thus, it is not surprising that we found by ^1H NMR that a series of aldehydes are generated upon cleavage of carbon–carbon double bonds in A2E following HRP-associated oxidation and degradation. The formation of aldehyde moieties (Figure 8) is also supported by the ^{18}O -labeling and NMR experiments (Figure 7e).

The mechanisms involved in HRP-mediated A2E cleavage, as described above, appear to be different from those we observed with A2E cleavage following photooxidation. In particular, photooxidation of A2E occurs primarily via singlet oxygen addition at C=C bonds to form endoperoxides, cleavage of which generates aldehyde or methylketone-bearing fragments.¹⁷ In the present work we focused on A2E, just one of the bisretinoids of RPE lipofuscin. Nevertheless, these findings are applicable to the other lipofuscin bisretinoids we have characterized (discussed above) since all of these compounds present with polyene side arms. Bisretinoids appears to be the major constituents of RPE lipofuscin since, when they do not form, the autofluorescence originating in RPE lipofuscin is absent.²⁴

CONCLUSION

In summary, we have found that HRP can degrade the bisretinoid A2E. This attempt at harnessing an exogenous enzyme to expand the catabolic function of cells is in some ways similar to enzyme replacement therapies aimed at reversing lysosomal storage diseases.²⁵ This venture is not the first to consider HRP for medical therapies. For example, it has been suggested that tumor-targeted HRP could be employed together with a prodrug to generate cytotoxic products for use in cancer therapy.²⁶ There is also interest in using HRP as a biocatalyst in the commercial production of drugs. Toward these ends, the HRP gene has been synthesized and expressed in *Escherichia coli*

and the chemistry of HRP has been successfully modified via site-directed mutagenesis.²⁷ Going forward we will examine additional enzyme candidates for their ability to degrade the bisretinoids of RPE lipofuscin along with delivery strategies that will specifically target the lysosomal organelles of RPE.

EXPERIMENTAL SECTION

Synthesis. A2E and bromine-tagged A2E (A2E-Br) were synthesized as previously described.^{1c,17}

Cell-Free Assays. A2E and A2E-Br (20 μM from a 10 mM stock in DMSO) were incubated with horseradish peroxidase (HRP type IV; 200 units/mL; Sigma-Aldrich Corp., St. Louis, MO) at room temperature in 500 μL of citrate buffer (pH 6.5; with 0.03% EDTA and 0.4% Tween 20) or water and with and without H_2O_2 (0.2–0.6%) for 3–24 h as indicated. In some experiments, A2E (20 μM) was also incubated in phosphate-buffered saline (with 0.2% DMSO) containing 200 units/mL cathepsin D (from human liver; Sigma-Aldrich Corp., St. Louis, MO) for 5 h at room temperature. Mixtures were extracted with chloroform, dried under argon, and analyzed by HPLC and UPLC–MS as described below.

Cell-Based Assays. A human adult RPE cell line (ARPE-19; American Type Culture Collection, Manassas, VA) that is devoid of endogenous A2E^{1c} was cultured in 35 mm cell culture dishes (Corning, NY) to confluence as previously reported.^{14,28} The cells were allowed to accumulate synthesized A2E^{1c} for 3 weeks from a 10 μM concentration in culture media^{9a} that included 10% fetal bovine serum (FBS; Invitrogen, Carlsbad, CA). Incubation of ARPE-19 cells with A2E at higher concentrations perturbs cell membranes.^{14,29} Following accumulation, the cells were allowed to quiesce for at least 3–7 days. Subsequently, HRP was delivered to the cells using a Bioporter protein delivery system (Sigma-Aldrich Corp., St. Louis, MO) as vehicle. Briefly, 100 ng of HRP in 40 μL of serum-free DMEM was combined with Bioporter reagent and, after mixing, was incubated at room temperature for 5 min. After bringing the final volume of the Bioporter/HRP mixture to 1 mL with serum-free medium, the mixture was added to the DMEM-washed cultures and incubated for 4 h at 37 °C after which FBS was added to a final concentration of 5% and incubation was continued for 20 h. Bioporter/HRP loading was repeated two additional times, and 2 days after the final Bioporter/HRP treatment, cells were harvested for HPLC analysis. Controls included cells incubated with Bioporter in the absence of HRP and cells not incubated.

Immunocytochemical Detection of HRP. ARPE-19 cells to which HRP was delivered via the Bioporter reagent were fixed with 4% paraformaldehyde for 15 min at room temperature, permeabilized with 0.1% Triton X-100, and washed with phosphate-buffered saline (three changes, 5 min each). The cultures were incubated with mouse anti-HRP antibody (Abcam, Cambridge, MA; 1:100 dilution) for 2 h at room temperature followed by biotinylated horse antimouse IgG (Vector Laboratories, Burlingame, CA) and then Vectastain ABC–alkaline phosphatase (Vector Laboratories). Vector Red (Vector Laboratories) was used as alkaline phosphatase substrate, generating a reaction product that can be viewed with both bright field and fluorescence microscopy.

To examine for colocalization of HRP and a lysosomal marker, ARPE-19 cells that had accumulated HRP by means of the Bioporter delivery system were incubated with 50 nM LysoTracker Red (Invitrogen, Carlsbad, CA) for 30 min at 37 °C. The cells were then fixed with 2% paraformaldehyde (Tousimis, Rockville, MD) and permeabilized with 0.2% Triton X-100 (Sigma-Aldrich, St. Louis, MO). After blocking with 5% normal goat serum the slide was incubated with mouse anti-HRP monoclonal antibody (Abcam, Cambridge, MA) followed by DyLight 488-conjugated affinity purified goat antimouse IgG (Jackson ImmunoResearch Laboratories, West Grove, PA). The cells were stained with DAPI (4',6-diamidino-2-phenylindole; Invitrogen, Carlsbad, CA)

before coverslipping. Images were captured with a Zeiss multiphoton confocal microscope (LSM 510 NLO; Carl Zeiss, Heidelberg, Germany) using 488 nm excitation and 500–550 nm emission for HRP, 543 nm excitation and 565–615 nm emission for LysoTracker Red, and two-photon excitation at 780 nm for DAPI with emission at 435–485 nm.

Cell Viability Assays. Cytotoxicity was assayed by MTT (4,5-dimethylthiazol-2-yl)-2,5-diphenyltetrazolium bromide) a colorimetric assay (Roche Diagnostics, Basel, Switzerland) that measures the ability of viable cells to cleave the yellow tetrazolium salt MTT to purple formazan crystals. Briefly, 20 μL of MTT reagent was added to 0.2 mL of culture medium in each well, and after incubating for 4 h, 200 μL of solubilization solution was added and incubation was continued overnight. After centrifugation, supernatants were measured spectrophotometrically, a decrease in the 570 nm absorbance indicating a loss in cellular viability.

Percent of nonviable cells was also determined by labeling the nuclei of nonviable cells with Dead Red (Molecular Probes, Eugene, OR) and nuclei of all cells with DAPI.³⁰ Values in each experiment were based on the sampling of five fields per well.

HPLC Quantitation. Samples were analyzed by reversed-phase HPLC using an Alliance System (Waters Corp., Milford, MA) equipped with 2695 separation module, 2996 photodiode array detector, and a 2475 multi- λ fluorescence detector. For chromatographic separation, an analytical scale Atlantis dC18 (3 μm , 4.6 mm \times 150 mm, Waters) column was utilized with an acetonitrile and water gradient and 0.1% trifluoroacetic acid (85–100%, 0.8 mL/min 15 min; 100% acetonitrile, 0.8–1.2 mL/min 15–20 min; monitoring at 430 nm; 30 μL injection volume). Extraction and injection for HPLC was performed under dim red light. Integrated peak areas were determined using Empower software, and picomolar concentrations were calculated by reference to an external standard of synthesized compound and by normalizing to the ratio of the HPLC injection volume versus total extract volume.

UPLC–MS Analysis. A2E-Br (3 μL of 10 mM stock in DMSO), which imparted enhanced sensitivity, or A2E was added to 500 μL of water containing 200 units/mL of HRP and 1 μL of H_2O_2 . This reaction mixture was incubated for 3 and 18 h at room temperature and then subjected to UPLC–MS using a Waters SQD single-quadrupole mass spectrometer that was coupled online to a Waters Acquity UPLC system (Waters, New Jersey) with a PDA e λ detector, sample manager, and binary solvent manager. The mass spectrometer was equipped with ESCi multimode ionization and an ion trap analyzer operating in full scan mode from m/z 200 to 1200. For compound elution, an Acquity BEH C18 (1.7 μm , 2.1 mm \times 50 mm) reversed-phase column was used for the stationary phase and for the mobile phase a gradient of acetonitrile in water with 0.1% formic acid: 50–70% acetonitrile (0–3 min); 70–100% acetonitrile (3–30 min) with a flow rate of 0.5 mL/min. Detection at 430 nm was by photodiode array.

¹⁸O-Labeled Assays. A2E-Br (20 μM) was incubated in 500 μL of ¹⁸O-labeled water (H_2^{18}O , 99 atom % ¹⁸O, Sigma-Aldrich) (with 0.2% DMSO) containing 200 units/mL HRP (type IV; Sigma-Aldrich Corp., St. Louis, MO) in the presence of 5 μL of ¹⁸O-labeled hydrogen peroxide ($\text{H}_2^{18}\text{O}_2$, 90 atom % ¹⁸O, Sigma-Aldrich) for 18 h at room temperature. Subsequently, the 10 μL of mixtures were analyzed by UPLC–MS as described above.

Statistical Analysis. Data were analyzed by one-way ANOVA and Newman–Keul multiple comparison test (Prism, GraphPad Software, San Diego, CA).

ASSOCIATED CONTENT

S Supporting Information. Additional supporting figures (Figures S1–S3) and the complete ref 4. This material is available free of charge via the Internet at <http://pubs.acs.org>.

AUTHOR INFORMATION

Corresponding Author

jrs88@columbia.edu

ACKNOWLEDGMENT

This work was supported by Grants from the Edward N. and Della L. Thome Memorial Foundation, National Institutes of Health Grant EY 12951 (J.R.S.), the Methusaleh Foundation, and unrestricted funds from Research to Prevent Blindness to the Department of Ophthalmology.

REFERENCES

- (1) (a) Fishkin, N.; Sparrow, J. R.; Allikmets, R.; Nakanishi, K. *Proc. Natl. Acad. Sci. U.S.A.* **2005**, *102*, 7091–7096. (b) Kim, S. R.; Jang, Y. P.; Jockusch, S.; Fishkin, N. E.; Turro, N. J.; Sparrow, J. R. *Proc. Natl. Acad. Sci. U.S.A.* **2007**, *104*, 19273–19278. (c) Parish, C. A.; Hashimoto, M.; Nakanishi, K.; Dillon, J.; Sparrow, J. R. *Proc. Natl. Acad. Sci. U.S.A.* **1998**, *95*, 14609–14613. (d) Wu, Y.; Fishkin, N. E.; Pande, A.; Pande, J.; Sparrow, J. R. *J. Biol. Chem.* **2009**, *284*, 20155–20166.
- (2) (a) Ben-Shabat, S.; Parish, C. A.; Vollmer, H. R.; Itagaki, Y.; Fishkin, N.; Nakanishi, K.; Sparrow, J. R. *J. Biol. Chem.* **2002**, *277*, 7183–7190. (b) Liu, J.; Itagaki, Y.; Ben-Shabat, S.; Nakanishi, K.; Sparrow, J. R. *J. Biol. Chem.* **2000**, *275*, 29354–29360.
- (3) Sparrow, J. R.; Kim, S. R.; Cuervo, A. M.; Bandhyopadhyay, U. *Adv. Exp. Med. Biol.* **2008**, *613*, 393–398.
- (4) Allikmets, R.; et al. *Nat. Genet.* **1997**, *15*, 236–246.
- (5) (a) Ahn, J.; Wong, J. T.; Molday, R. S. *J. Biol. Chem.* **2000**, *275*, 20399–20405. (b) Sun, H.; Molday, R. S.; Nathans, J. *J. Biol. Chem.* **1999**, *274*, 8269–8281.
- (6) (a) Shroyer, N. F.; Lewis, R. A.; Allikmets, R.; Singh, N.; Dean, M.; Leppert, M.; Lupski, J. R. *Vision Res.* **1999**, *39*, 2537–2544. (b) Weng, J.; Mata, N. L.; Azarian, S. M.; Tzekov, R. T.; Birch, D. G.; Travis, G. H. *Cell* **1999**, *98*, 13–23. (c) Wu, L.; Nagasaki, T.; Sparrow, J. R. *Adv. Exp. Med. Biol.* **2010**, *664*, 533–539.
- (7) Vasireddy, V.; Jablonski, M. M.; Khan, N. W.; Wang, X. F.; Sahu, P.; Sparrow, J. R.; Ayyagari, R. *Exp. Eye Res.* **2009**, *89*, 905–912.
- (8) (a) Maeda, A.; Maeda, T.; Sun, W.; Zhang, H.; Baehr, W.; Palczewski, K. *Proc. Natl. Acad. Sci. U.S.A.* **2007**, *104*, 19565–19570. (b) Chrispell, J. D.; Feathers, K. L.; Kane, M. A.; Kim, C. Y.; Brooks, M.; Khanna, R.; Kurth, I.; Huebner, C. A.; Gal, A.; Mears, A. J.; Swaroop, A.; Napoli, J. L.; Sparrow, J. R.; Thompson, D. A. *J. Biol. Chem.* **2009**, *284*, 21468–21477.
- (9) (a) Zhou, J.; Jang, Y. P.; Kim, S. R.; Sparrow, J. R. *Proc. Natl. Acad. Sci. U.S.A.* **2006**, *103*, 16182–16187. (b) Zhou, J.; Kim, S. R.; Westlund, B. S.; Sparrow, J. R. *Invest. Ophthalmol. Visual Sci.* **2009**, *50*, 1392–1399.
- (10) Anderson, D. H.; Radeke, M. J.; Gallo, N. B.; Chapin, E. A.; Johnson, P. T.; Curletti, C. R.; Hancox, L. S.; Hu, J.; Ebright, J. N.; Malek, G.; Hauser, M. A.; Rickman, C. B.; Bok, D.; Hageman, G. S.; Johnson, L. V. *Prog. Retinal Eye Res.* **2010**, *29*, 95–112.
- (11) (a) Allocca, M.; Doria, M.; Petrillo, M.; Colella, P.; Garcia-Hoyos, M.; Gibbs, D.; Kim, S. R.; Maguire, A. M.; Rex, T. S.; Di Vicino, U.; Cuttillo, L.; Sparrow, J. R.; Williams, D. S.; Bennett, J.; Auricchio, A. *J. Clin. Invest.* **2008**, *118*, 1955–1964. (b) Kong, J.; Kim, S. R.; Binley, K.; Pata, I.; Doi, K.; Mannik, J.; Zernant-Rajang, J.; Kan, O.; Iqbal, S.; Naylor, S.; Sparrow, J. R.; Gouras, P.; Allikmets, R. *Gene Ther.* **2008**, *15*, 1311–1320.
- (12) (a) Radu, R. A.; Han, Y.; Bui, T. V.; Nusinowitz, S.; Bok, D.; Lichter, J.; Widder, K.; Travis, G. H.; Mata, N. L. *Invest. Ophthalmol. Visual Sci.* **2005**, *46*, 4393–4401. (b) Maiti, P.; Kong, J.; Kim, S. R.; Sparrow, J. R.; Allikmets, R.; Rando, R. R. *Biochemistry* **2006**, *45*, 852–860. (c) Maeda, A.; Maeda, T.; Golczak, M.; Palczewski, K. *J. Biol. Chem.* **2008**, *283*, 26684–26693.
- (13) Rakoczy, P. E.; Zhang, D.; Robertson, T.; Barnett, N. L.; Papadimitriou, J.; Constable, I. J.; Lai, C. M. *Am. J. Pathol.* **2002**, *161*, 1515–1524.
- (14) Sparrow, J. R.; Parish, C. A.; Hashimoto, M.; Nakanishi, K. *Invest. Ophthalmol. Visual Sci.* **1999**, *40*, 2988–2995.
- (15) Zheng, X.; Lundberg, M.; Karlsson, A.; Johansson, M. *Cancer Res.* **2003**, *63*, 6909–6913.
- (16) Marques, C.; Pereira, P.; Taylor, A.; Liang, J. N.; Reddy, V. N.; Swzeda, L. I.; Shang, F. *FASEB J.* **2004**, *18*, 1424–1426.
- (17) Wu, Y.; Yanase, E.; Feng, X.; Siegel, M. M.; Sparrow, J. R. *Proc. Natl. Acad. Sci. U.S.A.* **2010**, *107*, 7275–7280.
- (18) Jang, Y. P.; Matsuda, H.; Itagaki, Y.; Nakanishi, K.; Sparrow, J. R. *J. Biol. Chem.* **2005**, *280*, 39732–39739.
- (19) Ahn, S. H.; Duffel, M. W.; Rosazza, J. P. N. *J. Nat. Prod.* **1997**, *60*, 1125–1129.
- (20) Ximenes, V. F.; Fernandes, J. R.; Bueno, V. B.; Catalani, L. H.; de Oliveira, G. H.; Machado, R. G. P. *J. Pineal Res.* **2007**, *42*, 291–296.
- (21) Maeda, T.; Maeda, A.; Matosky, M.; Okano, K.; Roos, S.; Tang, J.; Palczewski, K. *Invest. Ophthalmol. Visual Sci.* **2009**, *50*, 4917–4925.
- (22) (a) Kumar, D.; de Visser, S. P.; Sharma, P. K.; Derat, E.; Shaik, S. J. *Biol. Inorg. Chem.* **2005**, *10*, 181–189. (b) de Visser, S. P.; Ogliaro, F.; Sharma, P. K.; Shaik, S. *Angew. Chem., Int. Ed.* **2002**, *41*, 1947–1951.
- (23) van Rantwijk, F.; Sheldon, R. A. *Curr. Opin. Biotechnol.* **2000**, *11*, 554–564.
- (24) Katz, M. L.; Redmond, T. M. *Invest. Ophthalmol. Visual Sci.* **2001**, *42*, 3023–3030.
- (25) Brady, R. O. *Rejuvenation Res.* **2006**, *9*, 237–244.
- (26) Folkes, L. K.; Greco, O.; Dachs, G. U.; Stratford, M. R.; Wardman, P. *Biochem. Pharmacol.* **2002**, *63*, 265–272.
- (27) Smith, A. T.; Santama, N.; Dacey, S.; Edwards, M.; Bray, R. C.; Thorneley, R. N.; Burke, J. F. *J. Biol. Chem.* **1990**, *265*, 13335–13343.
- (28) Sparrow, J. R.; Nakanishi, K.; Parish, C. A. *Invest. Ophthalmol. Visual Sci.* **2000**, *41*, 1981–1989.
- (29) Sparrow, J. R.; Cai, B.; Jang, Y. P.; Zhou, J.; Nakanishi, K. *Adv. Exp. Med. Biol.* **2006**, *572*, 63–68.
- (30) Sparrow, J. R.; Zhou, J.; Ben-Shabat, S.; Vollmer, H.; Itagaki, Y.; Nakanishi, K. *Invest. Ophthalmol. Visual Sci.* **2002**, *43*, 1222–1227.
- (31) (a) de Visser, S. P.; Shaik, S.; Sharma, P. K.; Kumar, D.; Thiel, W. J. *Am. Chem. Soc.* **2003**, *125*, 15779–15788. (b) Derat, E.; Shaik, S. *J. Am. Chem. Soc.* **2006**, *128*, 8185–8198.